Engineering pore limiting diameter of metal-organic frameworks for benchmark separation of mono- and di-branched hexane isomers

Jingyi Zhou,[a,1] Xiao Han,[a,1] Tian Ke,[a] Jasper M. van Baten,[b] Zongbi Bao,[a,c] Zhiguo Zhang,[a,c] Rajamani Krishna, [b*] Qilong Ren,[a,c] Qiwei Yang[a,c*]

[a]Key Laboratory of Biomass Chemical Engineering of Ministry of Education, College of Chemical and Biological Engineering, Zhejiang University, 310027 Hangzhou, Zhejiang, China.

[b]Van't Hoff Institute for Molecular Sciences, University of Amsterdam, Science Park 904, 1098 XH Amsterdam, The Netherlands.

[c]Institute of Zhejiang University-Quzhou, 324000 Quzhou, Zhejiang, China.

[*]Corresponding author. Email: yangqw@zju.edu.cn (Q. Y.), r.krishna@contact.uva.nl (R. K.).

[1]These authors contributed equally to this work.

Experimental Section

Materials

All starting materials and solvents were commercially available and used without further purification.

Characterization methods

The thermal gravimetric analysis was performed on SDT650. Experiments were carried out using an alumina pan under nitrogen flow with a heating rate of 10 °C/min from room temperature to 750 °C. Powder X-ray diffraction (PXRD) data were collected on a PANalytical X'Pert diffractometer (Cu Kα, λ = 1.540598 Å) with a step size of 0.026° and 30 s/step measuring time. The range of 2θ was from 5° to 60°.

Single-component vapor-phase adsorption measurements

Before the adsorption isotherms test, the synthesized samples were washed with 10 mL DMF and 10 mL ethanol three times each, and then dried and degassed under high vacuum (< 1 Pa) at 473 K for 24 hours. Vapor-phase adsorption measurements were conducted on BELSORP MAX II vapor adsorption analyzer and about 50 mg of activated sample was used. The sorption isotherms of nHEX, 3MP and 22DMB were collected at 303, 333, 363 and 393 K. The kinetic adsorption data of nHEX, 3MP and 22DMB were also collected at 303, 333, 363 and 393 K.

Adsorption kinetics test

Adsorption kinetics tests were conducted on BELSORP MAX II vapor adsorption analyzer and about 50 mg of activated sample was used. A certain volume of vapor was introduced into the sample chamber, and the pressure in the sample chamber was recorded as a function of time, which was then converted into an instantaneous adsorption amount. To extract the intracrystalline diffusivity, a simplified micropore diffusion model was used. The mass transfer resistance in micropores is more important and the adsorbent crystals can be regarded as an approximately spherical object.

Recyclability tests

About 5 mg activated Mn_2TTFTB was held in the tube furnace of SDT650 under a nitrogen atmosphere at 333 K. A continuous total flow of vaporized nHEX, generated by flowing N_2 through metal bubblers containing the pure liquid nHEX, was introduced at a rate of 10 mL/min. The weight change of the sample was recorded. After equilibrium, the flow of vaporized nHEX was replaced with pure N_2, and the sample was heated from 333 K to 473 K and kept for 20 minutes to fully desorb the nHEX. Then, the tube furnace was cooled to 333 K and the adsorption-desorption steps were repeated thirty times.".

Multicomponent vapor-phase breakthrough experiments

Multicomponent vapor-phase breakthrough experiments were performed using a stainless steel column (4.6 mm inner diameter × 30 mm), which was packed with

activated MOF powder.[1] A continuous total flow of 1 mL/min, consisting of vaporized hexane isomers in nitrogen (N_2, 99.999%) was generated by flowing N_2 through metal bubblers containing the liquid components. By adjusting the ratio of each component in the liquid and the temperature of the bubbler, the partial pressure of hexane isomers carried by N_2 was the same, that is, the mole concentration was the same. The liquid volume composition and temperature of different bubblers were as follows: nHex:3MP:22DMB = 0.44:0.36:0.2, T=290.15 K; nHex: 22DMB = 0.69:0.31, T=281.15 K; 3MP:22DMB = 0.66:0.34, T=278.15 K. The partial pressure of each component was 47 torr. The gas stream at the outlet of the column was analyzed with a gas chromatograph (GC-9860, SSUN) with a flame ionization detector (FID). Breakthrough experiments were performed at 303, 333, 363 and 393 K. The dynamic adsorption capacity of hexane isomers was calculated from the breakthrough curve as in our earlier publications.[1] The di-branched isomer productivities are all calculated according to the formula: $p=(t_2-t_1) \times v \times c$; Here, p is the di-branched isomer productivity (in mmol/g); t_2 is the retention time of mono-branched isomer (min/g); t_1 is the retention time of di-branched isomer; v is the influent flow rate (mmol/min); c is the concentration of the specific vapor in the influent stream. After each breakthrough experiment, samples were regenerated and activated by purging with N_2 at 423 K for 48 h.

Density-functional theory calculations

The static binding energy was calculated using the combination of first-principle density functional theory (DFT) and plane-wave ultrasoft pseudopotential implemented in the Materials Studio, CASTEP code.[2] A semi-empirical addition of dispersive forces to conventional DFT was included in the calculation to account for van der Waals interactions. Calculations were performed under the generalized gradient approximation (GGA) with Perdew-Burke-Ernzerhof (PBE) exchange correlation.[2] A cutoff energy of 544 eV and 2×2×2 k-point mesh for M_2TTFTB (M=Zn, Mn, Cd) were found to be sufficient for total energy to converge within 0.02 mev/atom. Frameworks without guest molecules were first optimized. Then the isolated guest molecule was placed in the same cell dimensions as every sample crystal and was optimized and relaxed. Finally, various guest gas molecules were introduced to different locations of the channel pore and the whole structure was optimized as before. The static binding energy (at T=0 K) was then calculated: $\Delta E_{binding} = E(MOF) + E(guest) - E(MOF+guest)$.

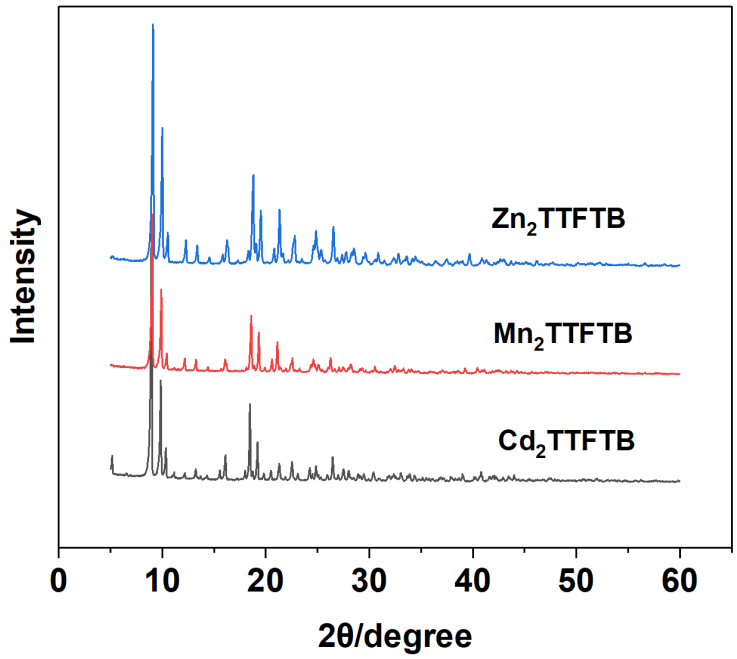

Fig. S1. PXRD patterns of as-synthesized M_2TTFTB (M=Zn, Mn, Cd).

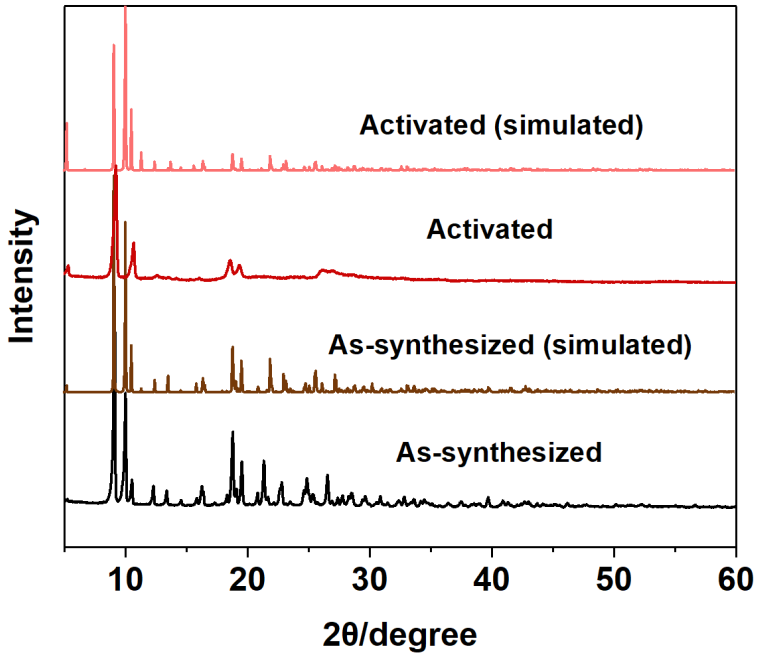

Fig. S2. PXRD patterns of as-synthesized and activated Zn_2TTFTB.

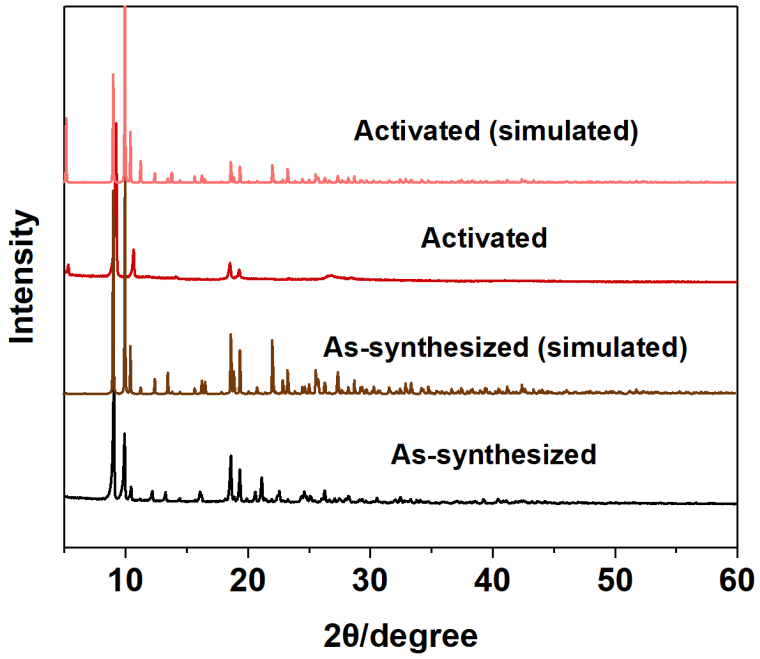

Fig. S3. PXRD patterns of as-synthesized and activated Mn_2TTFTB.

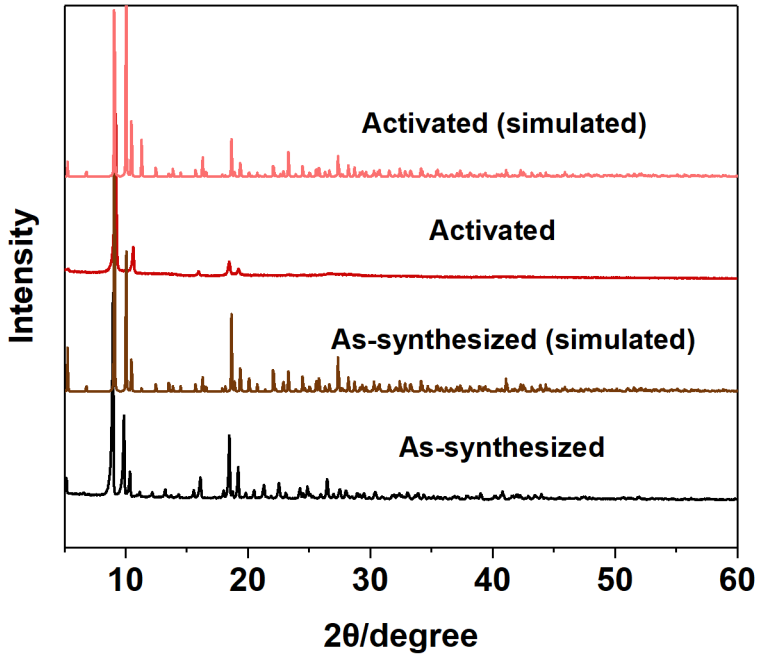

Fig. S4. PXRD patterns of as-synthesized and activated Cd_2TTFTB.

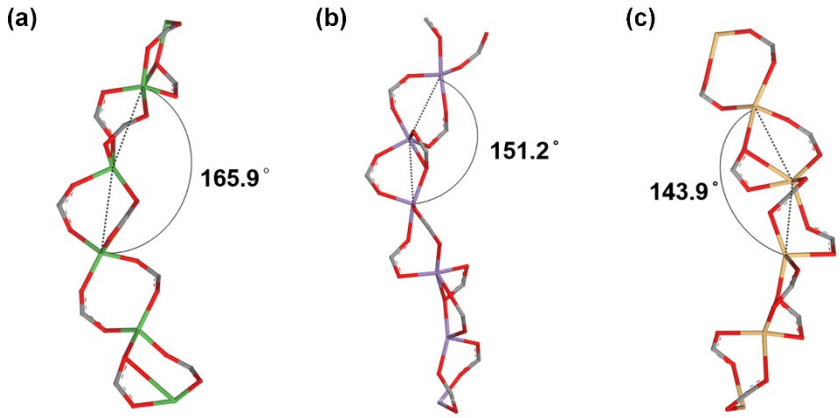

Fig. S5. Angles between adjacent metal atoms on infinite helical chains: (a) Zn_2TTFTB; (b) Mn_2TTFTB; (c) Cd_2TTFTB.

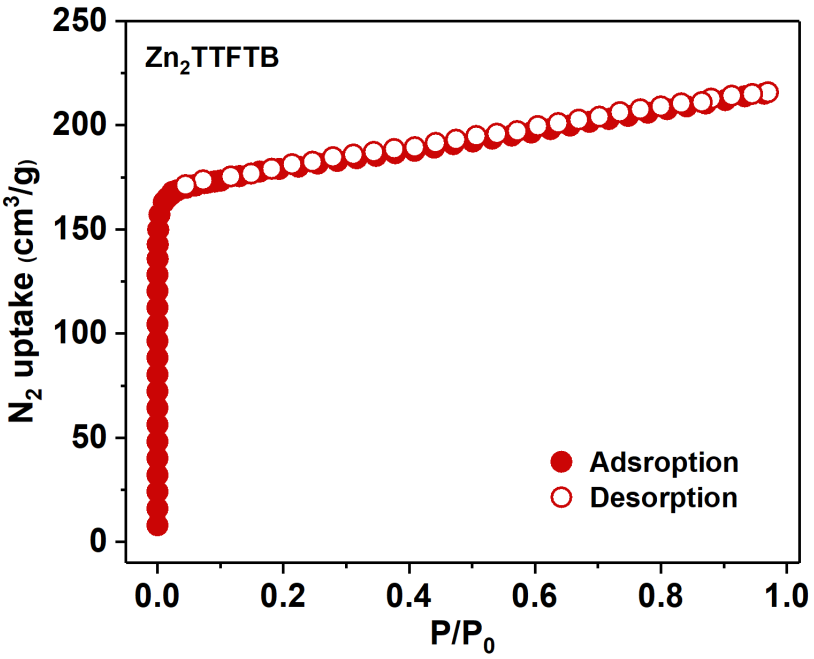

Fig. S6. The N_2 adsorption isotherms on Zn_2TTFTB at 77 K.

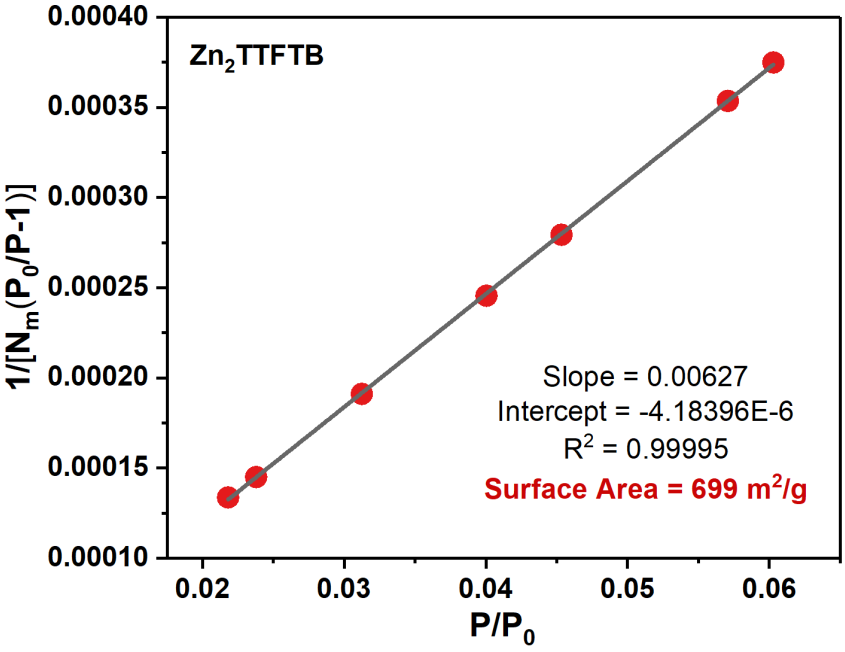

Fig. S7. Calculated BET surface area of Zn_2TTFTB.

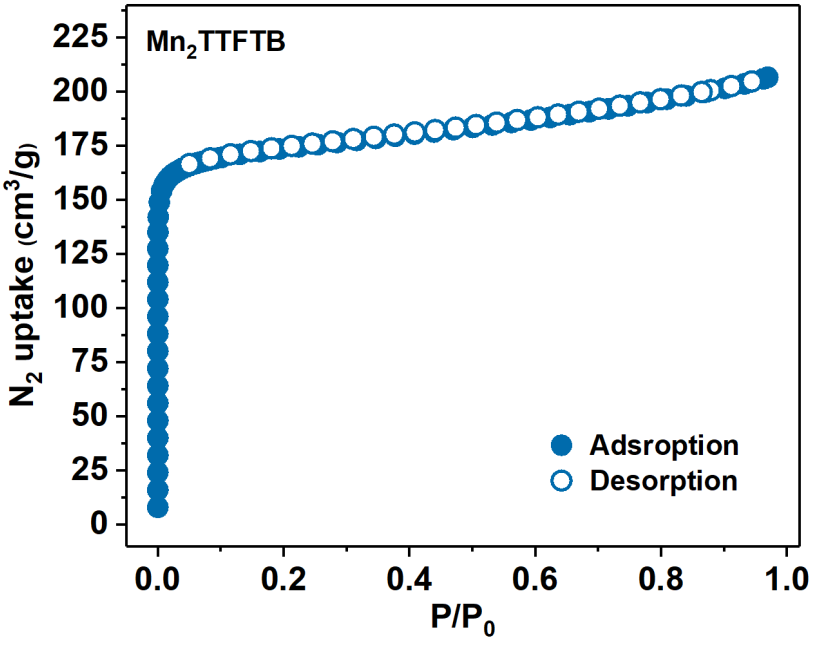

Fig. S8. The N_2 adsorption isotherms on Mn_2TTFTB at 77 K.

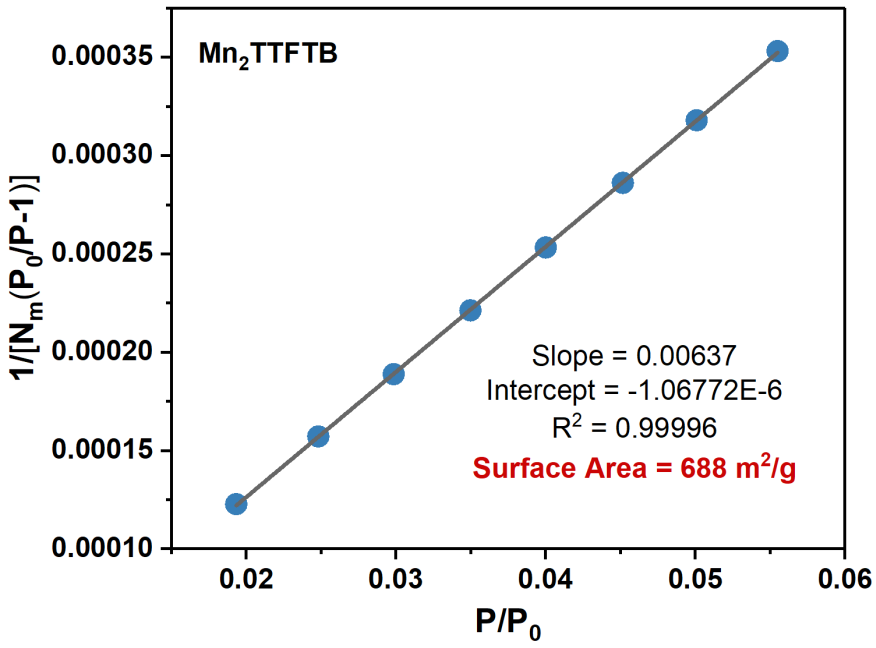

Fig. S9. Calculated BET surface area of Mn_2TTFTB.

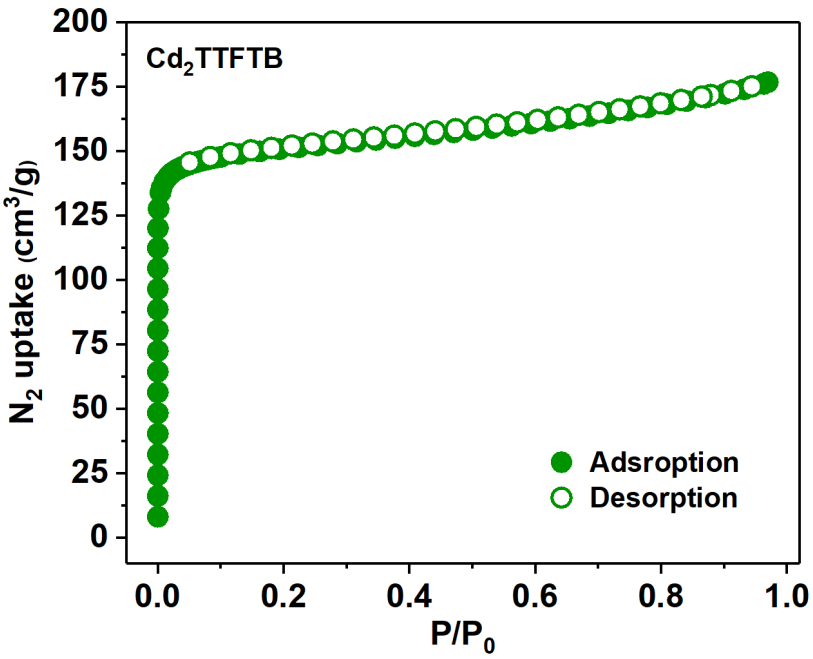

Fig. S10. The N_2 adsorption isotherms on Cd_2TTFTB at 77 K.

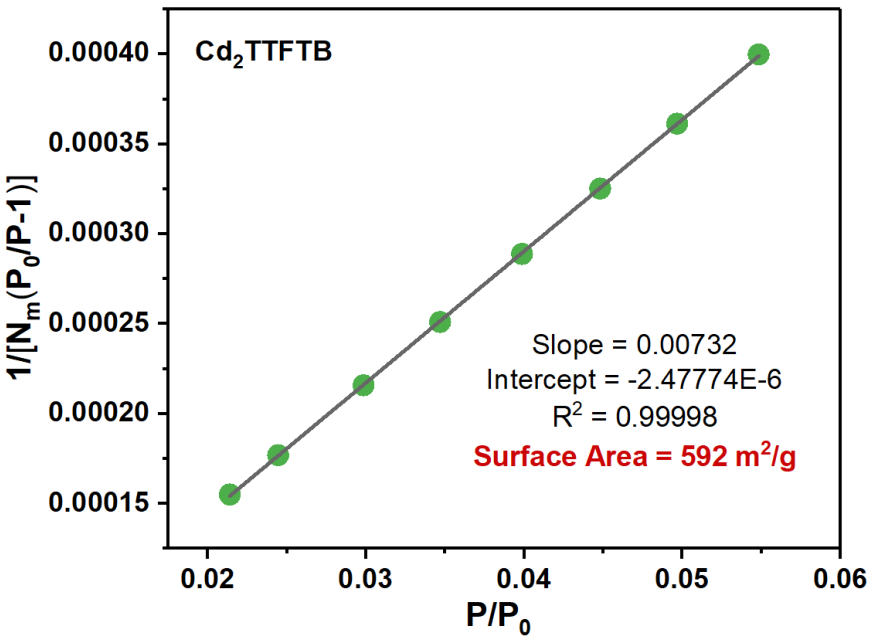

Fig. S11. Calculated BET surface area of Cd_2TTFTB.

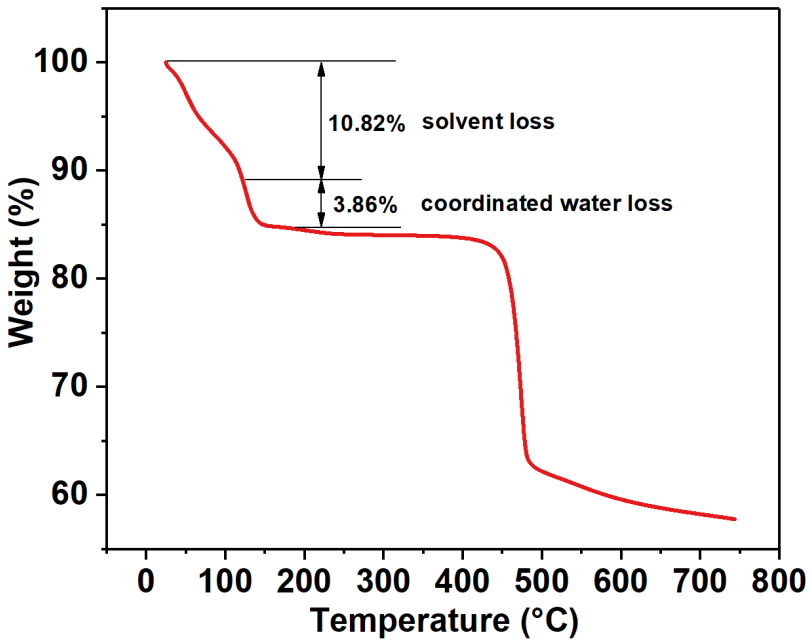

Fig. S12. The thermogravimetry curve of as-synthesized Zn_2TTFTB.

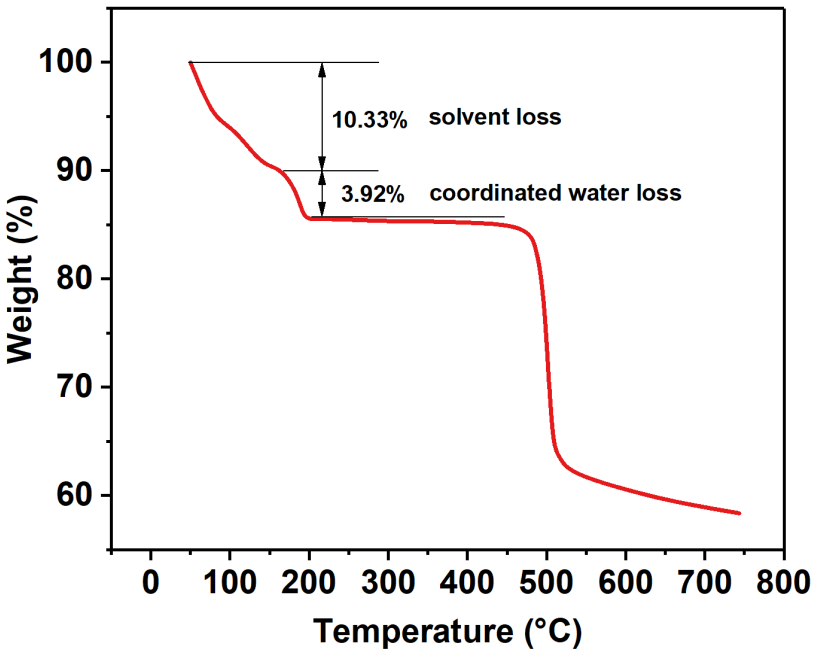

Fig. S13. The thermogravimetry curve of as-synthesized Mn_2TTFTB.

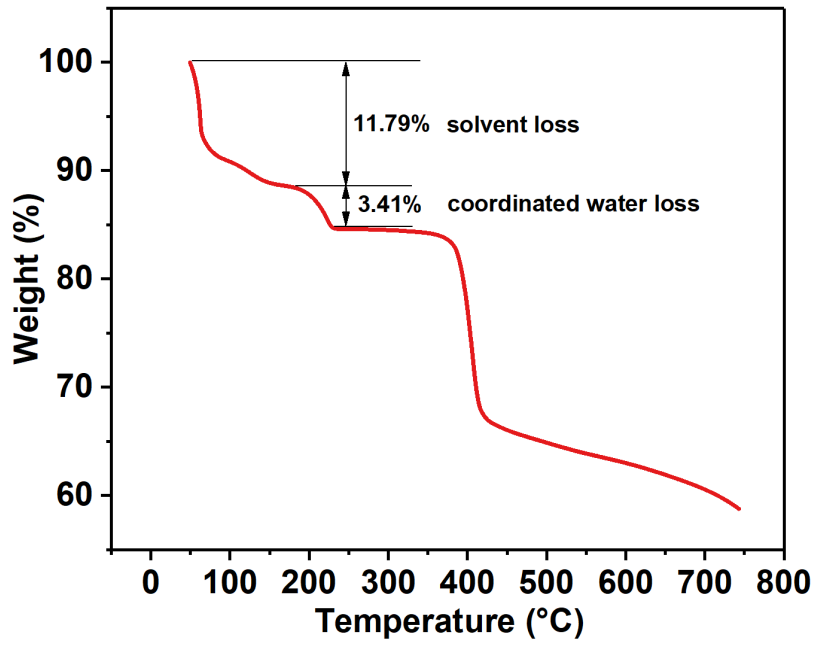

Fig. S14. The thermogravimetry curve of as-synthesized Cd_2TTFTB.

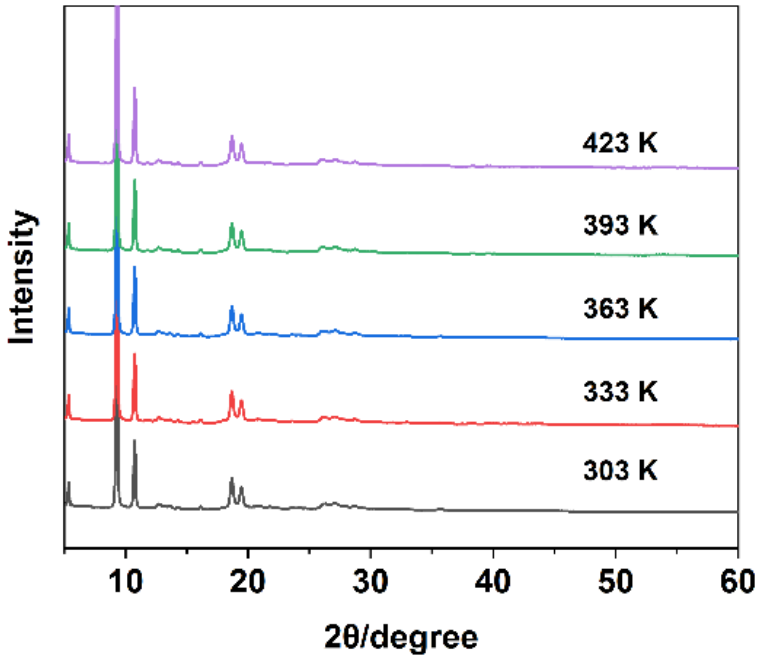

Fig. S15. In situ variable-temperature PXRD of Zn_2TTFTB.

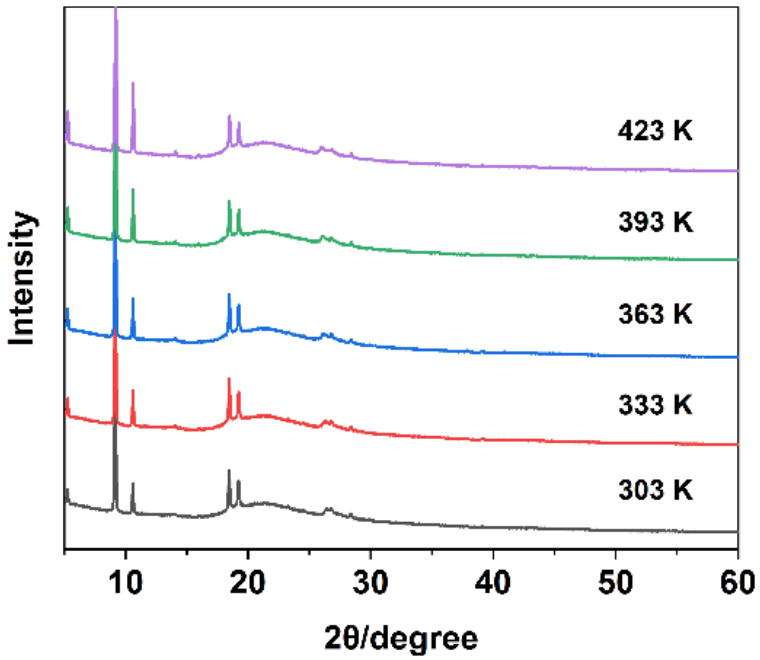

Fig. S16. In situ variable-temperature PXRD of Mn_2TTFTB.

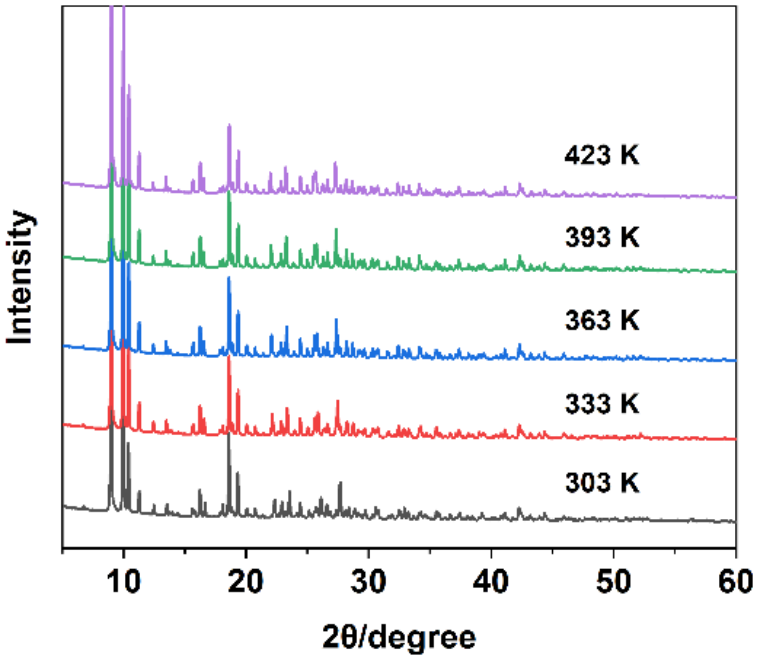

Fig. S17. In situ variable-temperature PXRD of Cd_2TTFTB.

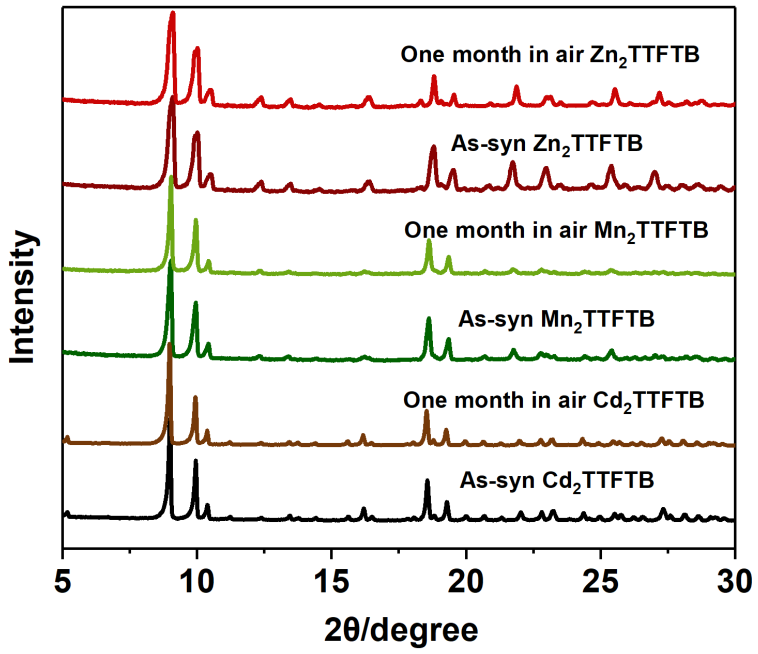

Fig. S18. PXRD patterns of M_2TTFTB (M=Zn, Mn, Cd) after exposure to air for one month.

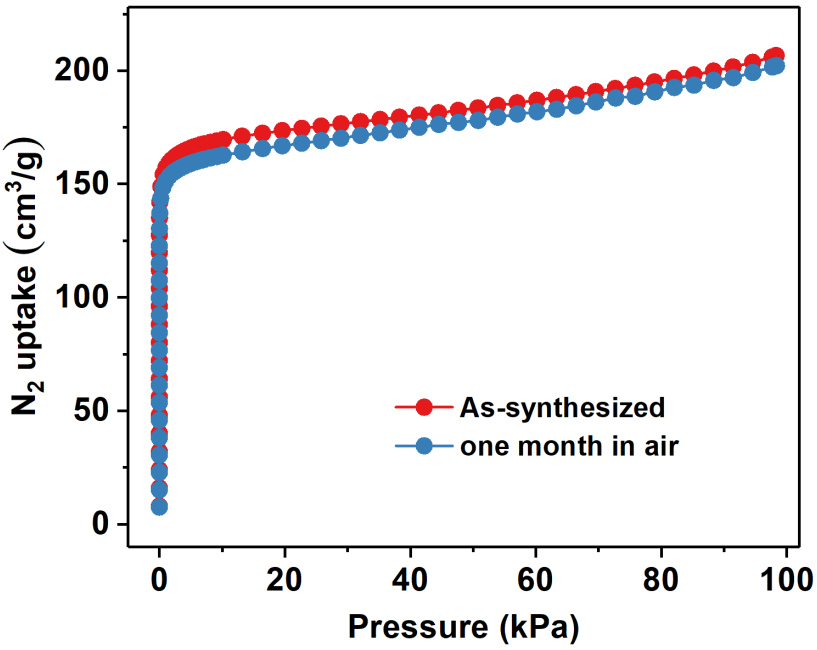

Fig. S19. The N_2 adsorption isotherms of Mn_2TTFTB after exposure to air for one month.

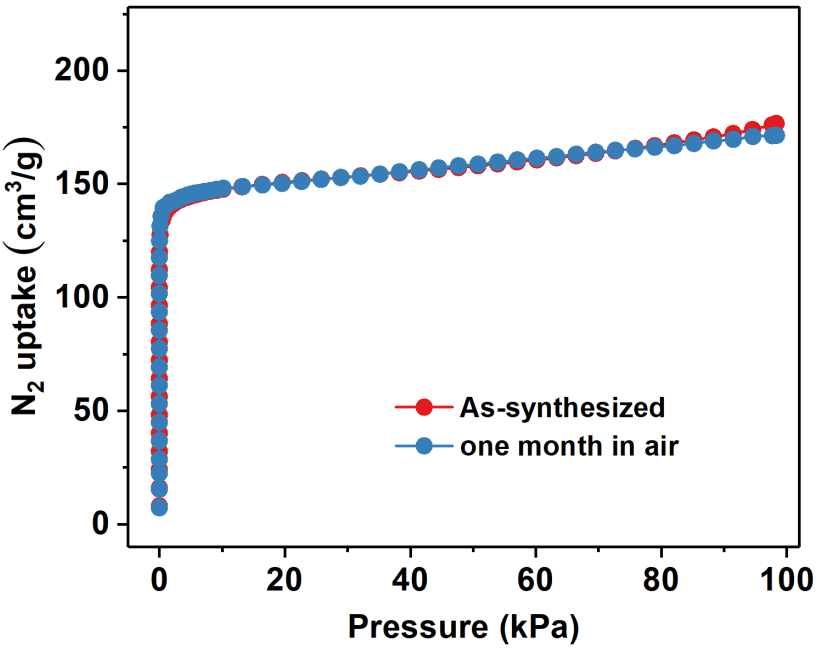

Fig. S20. The N_2 adsorption isotherms of Cd_2TTFTB after exposure to air for one month.

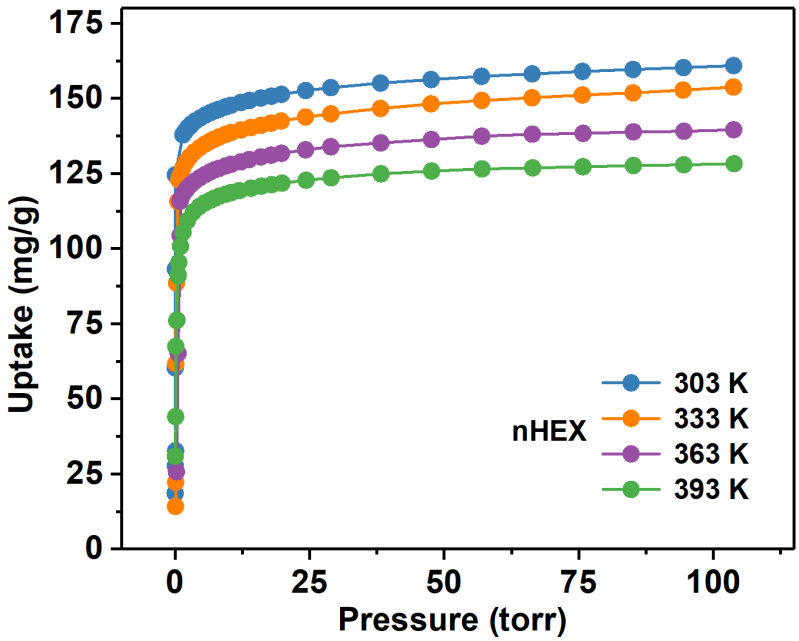

Fig. S21. The adsorption isotherms of nHEX on Zn_2TTFTB at different temperatures.

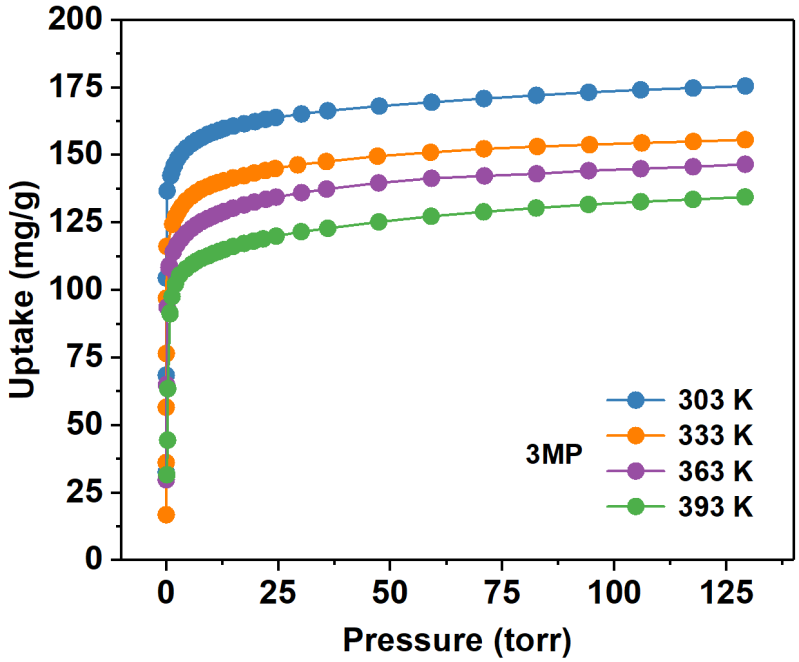

Fig. S22. The adsorption isotherms of 3MP on Zn_2TTFTB at different temperatures.

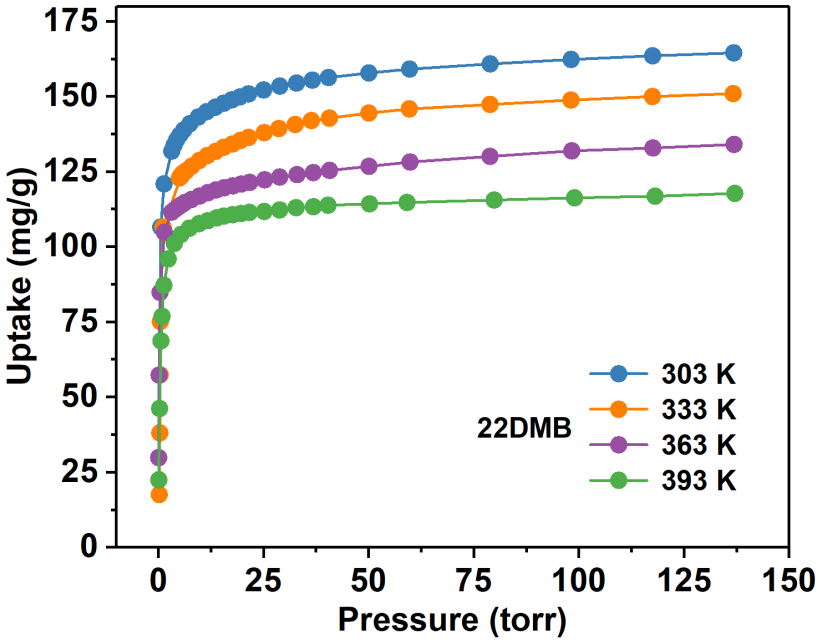

Fig. S23. The adsorption isotherms of 22DMB on Zn_2TTFTB at different temperatures.

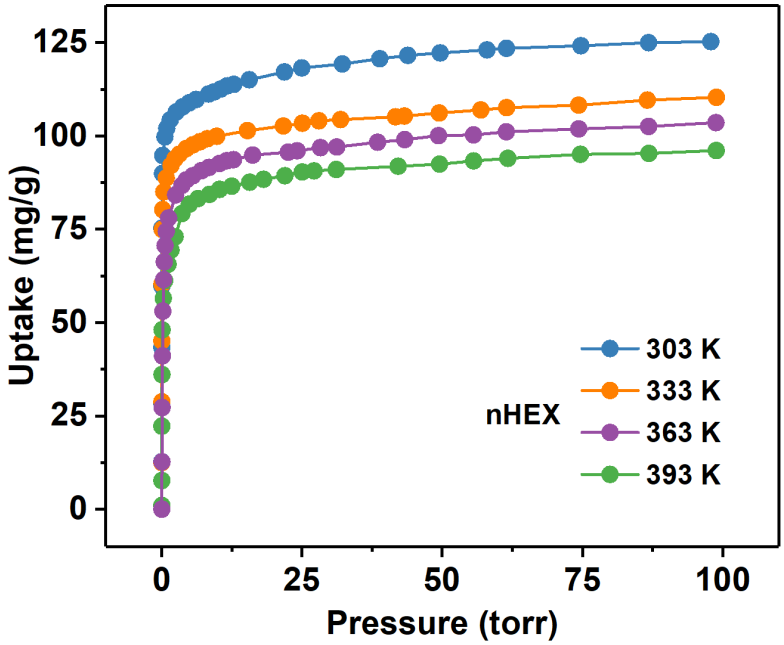

Fig. S24. The adsorption isotherms of nHEX on Cd_2TTFTB at different temperatures.

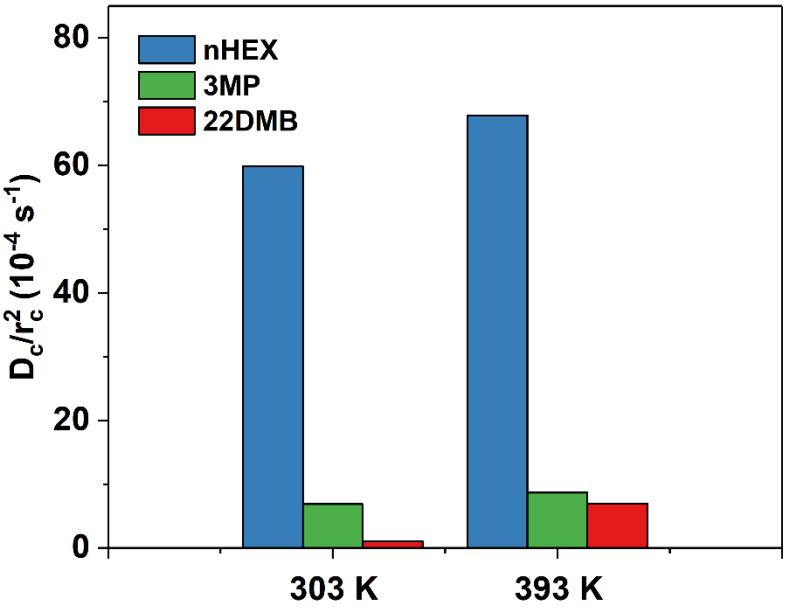

Fig. S25. Diffusion time constants of nHEX, 3MP and 22DMB on Zn_2TTFTB at 303 K and 393 K.

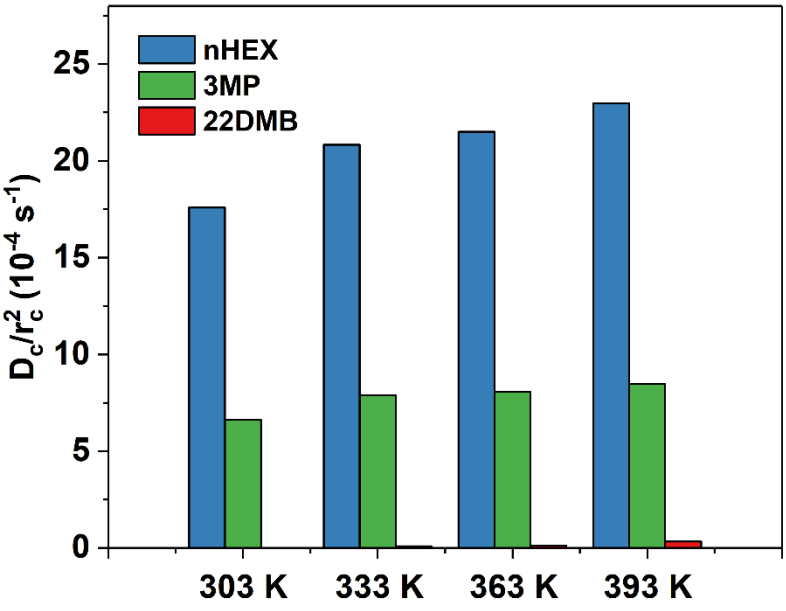

Fig. S26. Diffusion time constants of nHEX, 3MP and 22DMB on Mn_2TTFTB at 303 K, 333 K, 363 K and 393 K.

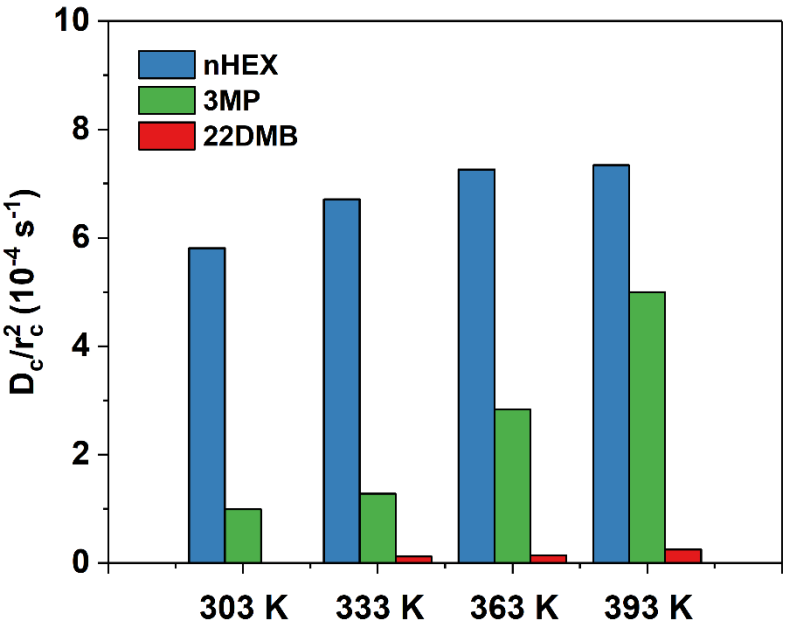

Fig. S27. Diffusion time constants of nHEX, 3MP and 22DMB on Cd_2TTFTB at 303 K, 333 K, 363 K and 393 K.

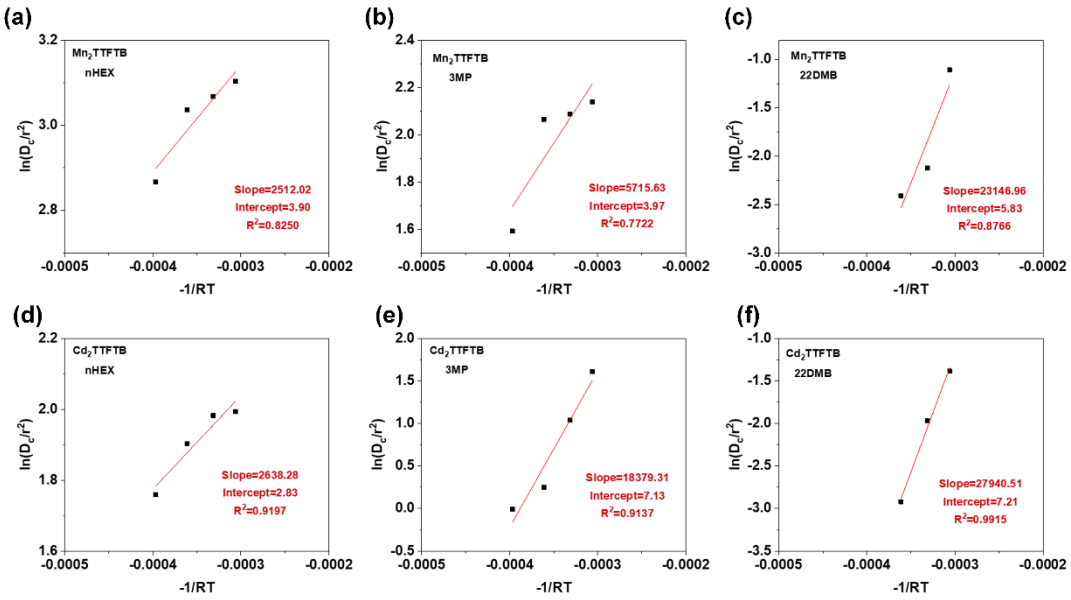

Fig. S28. Diffusion activation energy fitting curves of (a) nHEX, (b) 3MP, (c) 22DMB in Mn_2TTFTB, (d) nHEX, (e) 3MP, (f) 22DMB in Cd_2TTFTB.

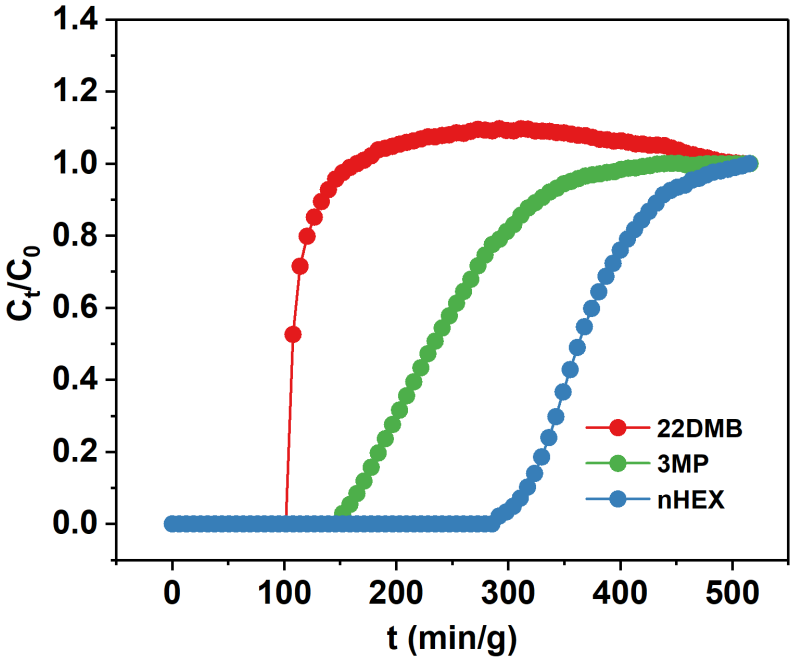

Fig. S29. Equimolar three-component vapor-phase breakthrough tests with partial pressure of 46 torr for each hexane isomer on Zn_2TTFTB at 303 K.

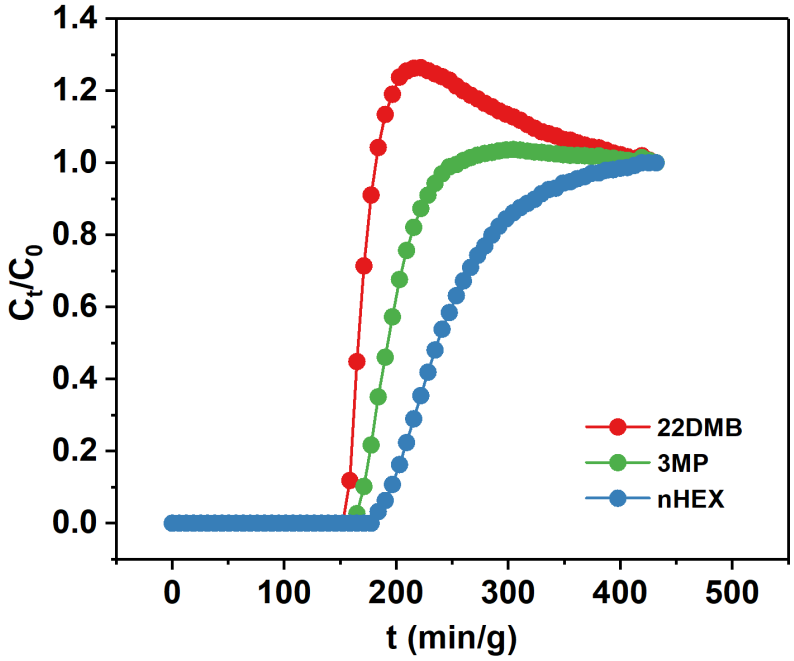

Fig. S30. Equimolar three-component vapor-phase breakthrough tests with partial pressure of 46 torr for each hexane isomer on Zn_2TTFTB at 393 K.

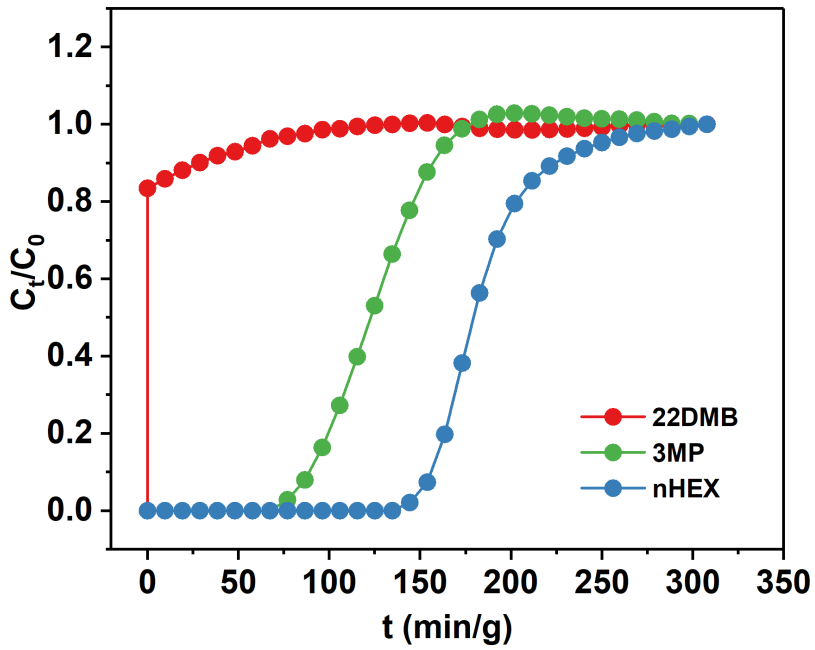

Fig. S31. Equimolar three-component vapor-phase breakthrough tests with partial pressure of 46 torr for each hexane isomer on Mn_2TTFTB at 303 K.

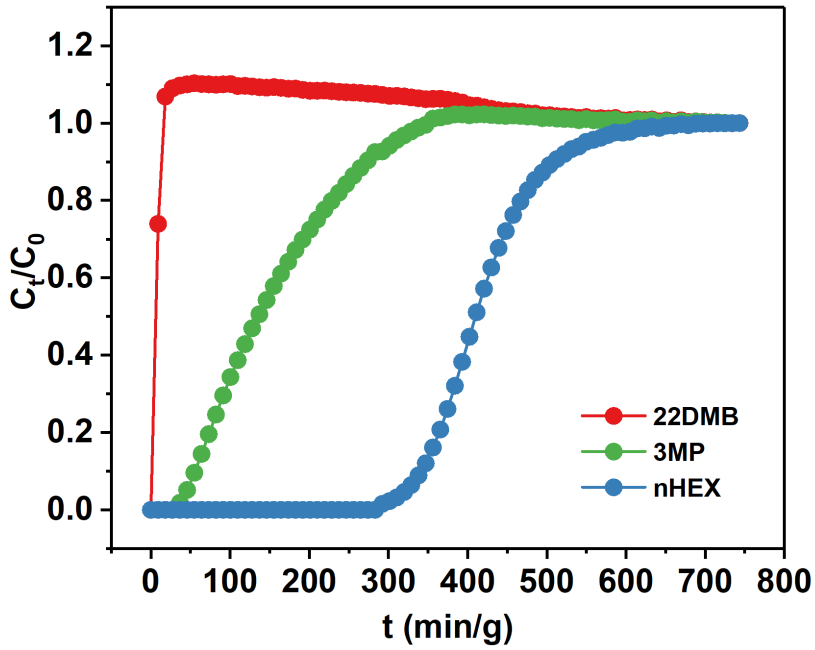

Fig. S32. Equimolar three-component vapor-phase breakthrough tests with partial pressure of 46 torr for each hexane isomer on Cd_2TTFTB at 303 K.

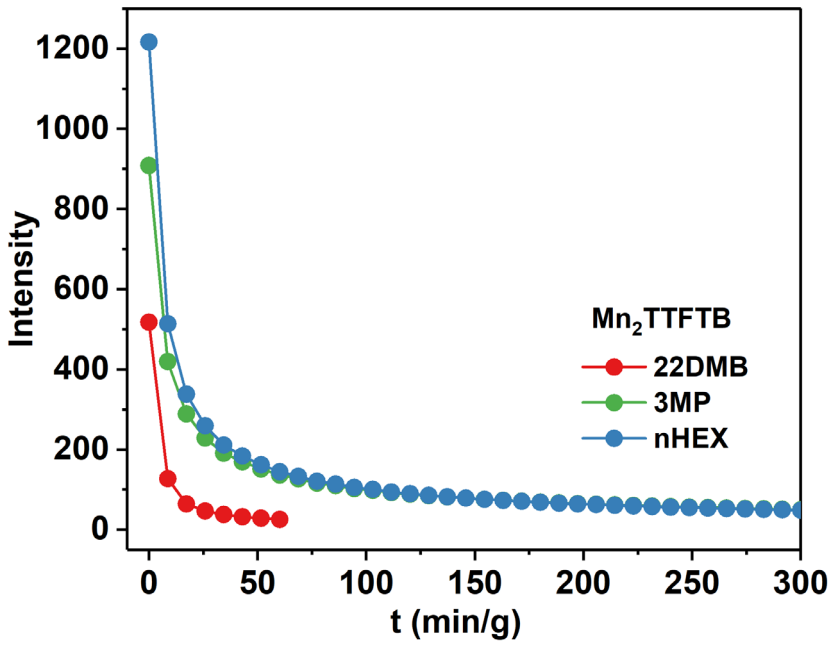

Fig. S33. The signals of desorbed hexane isomers in Mn_2TTFTB at 423 K.

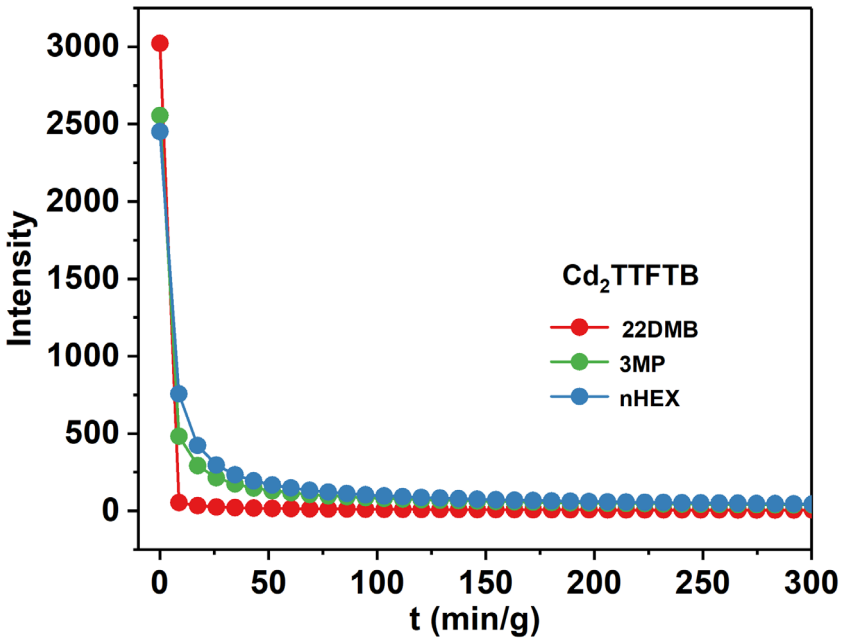

Fig. S34. The signals of desorbed hexane isomers in Cd_2TTFTB at 423 K.

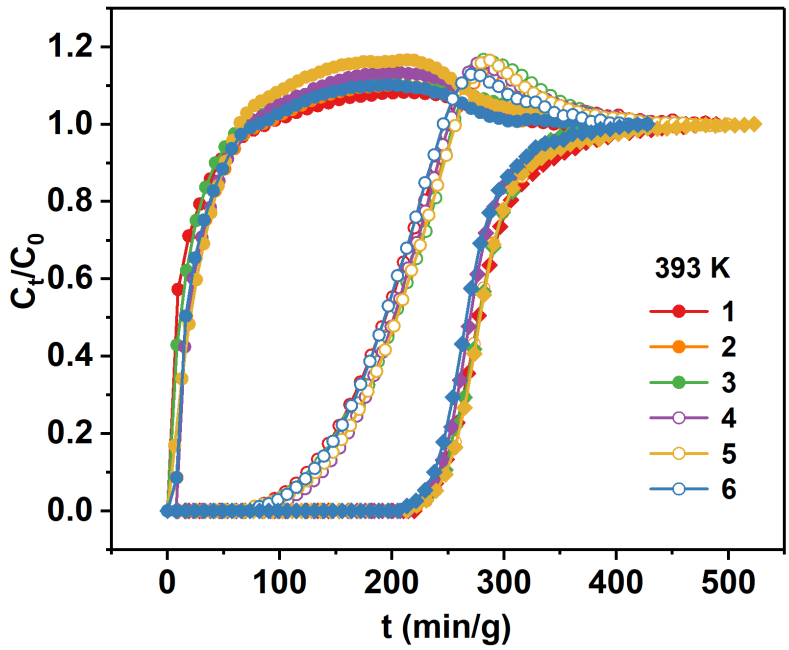

Fig. S35. Cycling test of the separation of equimolar ternary vapor-phase hexane isomers at 393 K with Mn_2TTFTB.

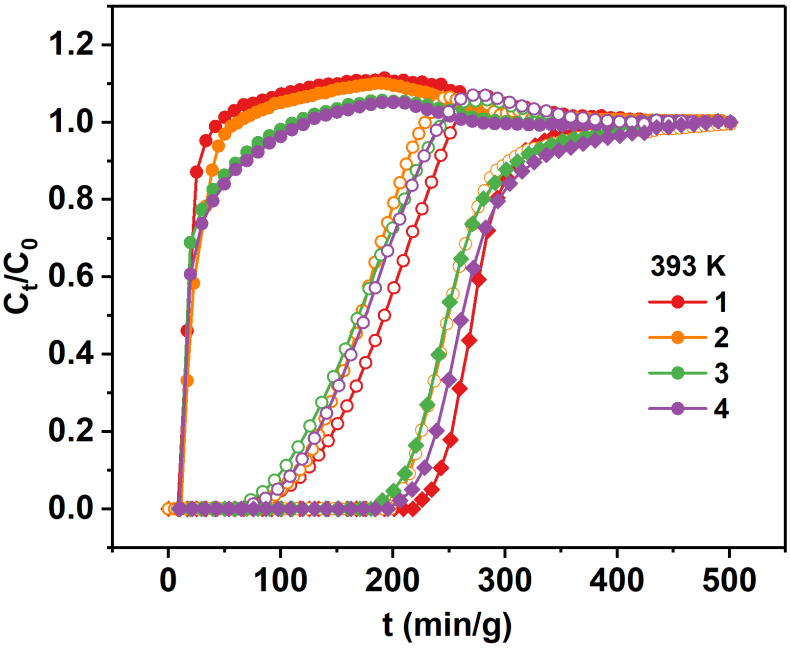

Fig. S36. Cycling test of the separation of equimolar ternary vapor-phase hexane isomers at 393 K with Cd_2TTFTB.

Table S1. Dynamic adsorption capacity and productivity of pure 22DMB (>99.9%) in breakthrough experiments for M_2TTFTB (M=Mn, Cd, Zn).

Adsorbent	T (K)	Dynamic capacity (mmol/g)			Productivity of 22DMB (mmol/g)
		nHEX	3MP	22DMB	
Zn_2TTFTB	303	0.98	0.70	0.18	0.11
	393	0.54	0.53	0.33	0.01
Mn_2TTFTB	303	0.53	0.29	0.00	0.17
	333	0.98	0.73	0.00	0.45
	363	0.74	0.56	0.00	0.31
	393	0.78	0.47	0.00	0.21
Cd_2TTFTB	303	1.19	0.36	0.00	0.07
	333	1.18	0.41	0.00	0.11
	363	0.95	0.73	0.00	0.36
	393	0.80	0.55	0.01	0.16

Table S2. Adsorptive separation of hexane isomers on various materials.

Adsorbent	Mechanism	*T*/K	Unary static adsorption uptake /mmol·g^{-1}	static adsorption pressure /torr	Di-branched isomer productivity/ mmol·g^{-1} [②]
Zr-bptc[14]	Molecular sieving	303	nHEX (1.89), 3MP, 23DMB	113	0
		423	nHEX (1.48), 3MP (0.29), 23DMB (0)		0
Zr-abtc[14]	Thermodynamic	303	nHEX (2.49), 3MP (2.08), 23DMB	98	0.59
		423	nHEX (1.21), 3MP (1.02), 23DMB (0.58)		0.10
Ca(H_2tcpb)[15]	Molecular sieving	303	nHEX (1.72), 3MP (1.91), 22DMB (1.16)	90	/
		333	nHEX (1.62), 3MP (1.39), 22DMB (0.09)		0.40
		393	nHEX (1.14), 3MP (0.08), 22DMB (0)		/
Al-bttotb[16]	Molecular sieving	303	nHEX (1.74), 3MP (1.08), 22DMB (0.11)	P_0[①]	0.23
$Fe_2(BDP)_3$[17]	Thermodynamic	433	nHEX (1.32), 2MP (1.07), 3MP (1.24), 23DMB (1.01), 22DMB (0.99)	98	/
$Fe_3(\mu_3$-O)$(6fdca)_3$[18]	Kinetic	298	nHEX (0.75), 3MP (0.65), 22DMB (0.05)	98	/
ZIF-8[19]	Kinetic	373	nHEX (2.25), 2MP (1.83), 23DMB (0.65), 22DMB (0.08)	113	/
MIL-53(Fe)-$(CF_3)_2$[20]	Kinetic	313	nHEX (0.37), 3MP (0.35), 22DMB (0.31)	P_0[①]	0.02
5A[21]	Molecular sieving	303	nHEX (1.21), 3MP (0.1)	113	0
HIAM-302[22]	Molecular sieving	298	nHEX (1.91), 3MP (1.09), 22DMB (0)	P_0[①]	0.12
CAU-10-H/Br[23]	Molecular sieving	303	nHEX (1.51), 3MP (0.75), 22DMB (0.12)	100	0.22
		333	nHEX (1.30), 3MP (0.76), 22DMB (0.10)		0.33
		363	nHEX (1.06), 3MP (0.75), 22DMB (0.12)		0.34
NU-2200[24]	Thermodynamic	298	nHEX (1.32), 2MP (1.03), 3MP (0.89), 23DMB (0.21), 22DMB (0.17)	120	/
NU-2002[25]	Thermodynamic	298	nHEX (1.41), 2MP (1.54), 3MP (1.56), 23DMB (1.67), 22DMB (1.31)	120	/
Mn_2TTFTB	Kinetic	303	nHEX (2.11), 3MP (2.41), 22DMB (0.65)	100	0.17
		333	nHEX (1.96), 3MP (2.20), 22DMB (1.06)		0.45
		363	nHEX (1.84), 3MP (2.02), 22DMB (0.96)		0.31
		393	nHEX (1.68), 3MP (1.82), 22DMB (0.83)		0.21
Cd_2TTFTB	Kinetic	303	nHEX (1.45), 3MP (1.72), 22DMB (0.84)	100	0.07
		333	nHEX (1.28), 3MP (1.53), 22DMB (1.20)		0.11
		363	nHEX (1.20), 3MP (1.31), 22DMB (1.31)		0.36
		393	nHEX (1.12), 3MP (1.38), 22DMB (1.02)		0.16
Zn_2TTFTB	Kinetic	303	nHEX (1.86), 3MP (2.01), 22DMB (1.88)	100	0.11
		393	nHEX (1.48), 3MP (1.53), 22DMB (1.35)		0.01

[①]The value of P_0 was not provided in the paper. [②]Calculated according to breakthrough curves

Table S3. Static adsorption energy of hexane isomers in M_2TTFTB (M=Zn, Mn, Cd).

Adsorbent	Static adsorption energy (kJ/mol)		
	nHEX	3MP	22DMB
Zn_2TTFTB	75.19	72.33	68.88
Mn_2TTFTB	80.15	77.19	72.44
Cd_2TTFTB	75.22	76.59	70.04

References

1 M. D. Segall, P. J. D. Lindan, M. J. Probert, C. J. Pickard, P. J. Hasnip, S. J. Clark, M. C. Payne, First-principles simulation: ideas, illustrations and the CASTEP code. J. Phys.-Condes. 14 (2002) 2717-2744.

2. R. Krishna, J. M. van Baten, In silico screening of metal-organic frameworks in separation applications. Phys. Chem. Chem. Phys. 13 (2011) 10593-10616.
3. R. Krishna, J. M. van Baten, In silico screening of zeolite membranes for CO_2 capture. J. Membr. Sci. 360 (2010) 323-333.
4. R. Krishna, J. M. van Baten, Describing mixture diffusion in microporous materials under conditions of pore saturation. J. Phys. Chem. C. 114 (2010) 11557-11563.
5. R. Krishna, J. M. van Baten, Diffusion of alkane mixtures in zeolites. Validating the Maxwell-Stefan formulation using MD simulations. J. Phys. Chem. B. 109 (2005) 6386-6396..
6. R. Krishna, J. M. van Baten, Insights into diffusion of gases in zeolites gained from molecular dynamics simulations. Microporous Mesoporous Mater. 109 (2008) 91-108.
7. R. Krishna, Describing the diffusion of guest molecules inside porous structures. J. Phys. Chem. C, 113 (2009) 19756-19781.
8. R. Krishna, Diffusion in porous crystalline materials. Chem. Soc. Rev. 41 (2012) 3099-3118.
9. D. Dubbeldam, S. Calero, T. J. H. Vlugt, R. Krishna, T. L. Maesen, B. Smit, United atom forcefield for alkanes in nanoporous materials. J. Phys. Chem. B, 108 (2004) 12301-12313.
10. D. Frenkel, B. Smit, Understanding molecular simulations: from algorithms to applications. 2nd Edition, Academic Press: San Diego, 2002.
11. W. Smith, T. R. Forester, I. T. Todorov, The DL_POLY Molecular Simulation Package. http://www.cse.clrc.ac.uk/msi/software/DL_POLY/index.shtml, Warrington, England, March 2006.
12. Rappé, A. K.; Casewit, C. J.; Colwell, K. S.; Goddard III, W. A.; Skiff, W. M. A full periodic table force field for molecular mechanics and molecular dynamics simulations. J. Am. Chem. Soc. 114 (1992) 10024-10035.
13. Mayo, S. L., Olafson, B. D., Goddard, W. J. DREIDING: A generic force field for molecular simulations. Phys. Chem. 94 (1990) 8897-8909.
14. H. Wang, X. Dong, J. Lin, S. J. Teat, S. Jensen, J. Cure, E. V. Alexandrov, Q. Xia, K. Tan, Q. Wang, D. H. Olson, Davide M. Proserpio, Y. J. Chabal, T. Thonhauser, J. Sun, Y. Han, J. Li, Topologically guided tuning of Zr-MOF pore structures for highly selective separation of C6 alkane isomers. Nat. Commun. 9 (2018) 1745.
15. H. Wang, X. Dong, E. Velasco, D. H. Olson, Y. Han, J. Li, One-of-a-kind: a microporous metal-organic framework capable of adsorptive separation of linear, mono- and di-branched alkane isomers via temperature- and adsorbate-dependent molecular sieving. Energy Environ. Sci. 11 (2018) 1226-1231.
16. L. Yu, X. Dong, Q. Gong, S. R. Acharya, Y. Lin, H. Wang, Y. Han, T. Thonhauser, J. Li, Splitting mono- and dibranched alkane isomers by a robust aluminum-based metal-organic framework material with optimal pore dimensions. J. Am. Chem. Soc. 142 (2020) 6925-6929.
17. Z. R. Herm, B. M. Wiers, J. A. Mason, J. M. van Baten, M. R. Hudson, P. Zajdel, C. M. Brown, N. Masciocchi, R. Krishna, J. R. Long, Separation of hexane isomers in a metal-organic framework with triangular channels. Science 340 (2013) 960-964.
18. D. Lv, H. Wang, Y. Chen, F. Xu, R. Shi, Z. Liu, X. Wang, S. J. Teat, Q. Xia, Z. Li, Iron-based metal-organic framework with hydrophobic quadrilateral channels for highly selective separation of hexane isomers. ACS Appl. Mater. Interfaces 10 (2018) 6031-6038.
19. A. F. Ferreira, M. C. Mittelmeijer-Hazeleger, M. A. Granato, V. F. Martins, A. E. Rodrigues, G. Rothenberg, Sieving di-branched from mono-branched and linear alkanes using ZIF-8: experimental proof and theoretical explanation. Phys. Chem. Chem. Phys. 15 (2013) 8795-8804.
20. P. A. P. Mendes, P. Horcajada, S. Rives, H. Ren, A. E. Rodrigues, T. Devic, E. Magnier, P. Trens, H. Jobic, J. Ollivier, G. Maurin, C. Serre, J. A. C. Silva. A complete separation of hexane isomers by a functionalized flexible metal organic framework. Adv. Funct. Mater. 24 (2014) 7666-7673.
21. D. Peralta, G. Chaplais, Simon-Masseron, A., K. Barthelet, G. D.Pirngruber, Separation of C6 paraffins using zeolitic imidazolate frameworks: Comparison with zeolite 5A. Ind. Eng. Chem. Res. 51 (2012) 4692-4702.
22. L. Yu, S. Ullah, K. Zhou, Q. Xia, H. Wang, S. Tu, J. Huang, H. L. Xia, X. Y. Liu, T. Thonhauser, A microporous metal-organic framework incorporating both primary and secondary building units for splitting alkane isomers. J. Am. Chem. Soc. 144 (2022) 3766-3770.
23. Q. Yu, L. Guo, D. Lai, Z. Zhang, Q. Yang, Y. Yang, Q. Ren, Z. Bao, A pore-engineered metal-organic framework with mixed ligands enabling highly efficient separation of hexane isomers for gasoline upgrading. Sep. Purif. Technol. 268 (2021) 118646.
24. B. Lal, K. B. Idrees, H. Xie, C. S. Smoljan, S. Shafaie, T. Islamoglu, O. K. Farha, Pore aperture control toward size-exclusion-based hydrocarbon separations. Angew. Chem. Int. Edit. 62 (2023) e202219053.
25. C. S. Smoljan, Z. Li, H. Xie, C. J. Setter, K. B. Idrees, F. A. Son, F. Formalik, S. Shafaie, T. Islamoglu, L. K. Macreadie, Engineering metal-organic frameworks for selective separation of hexane isomers using 3-dimensional linkers. J. Am. Chem. Soc. 145 (2023) 6434-6441.